Water Research 174 (2020) 115643

Contents lists available at ScienceDirect

Water Research

journal homepage: www.elsevier.com/locate/watres

Photocatalytic degradation of organic micropollutants: Inhibition mechanisms by different fractions of natural organic matter

Dion Awfa [a, b, **], Mohamed Ateia [c, *], Manabu Fujii [a], Chihiro Yoshimura [a]

[a] Department of Civil and Environmental Engineering, School of Environment and Society, Tokyo Institute of Technology, 2-12-1, M1-4, Ookayama, Meguro-ku, Tokyo, 152-8552, Japan
[b] Water and Wastewater Engineering Research Group, Faculty of Civil and Environmental Engineering, Institut Teknologi Bandung, Jl. Ganesha 10, Bandung, 40132, Indonesia
[c] Department of Chemistry, Northwestern University, Evanston, IL, 60208, United States

ARTICLE INFO

Article history:
Received 5 December 2019
Received in revised form
15 February 2020
Accepted 21 February 2020
Available online 24 February 2020

Keywords:
TiO_2
Carbon nanotubes
Natural organic matter
Inhibition
Organic micropollutants
Photocatalysis

ABSTRACT

Natural organic matter (NOM) can inhibit the photocatalytic degradation of organic micropollutants (OMPs) through inner filter effect, reactive oxygen species (ROS) scavenging, and competitive adsorption. However, previous studies have focused solely on the bulk properties of NOM and our understanding of the inhibition mechanism by NOM fractions during photocatalytic degradation of OMP is still fragmentary. In this study, five well-characterized different NOM samples (i.e., secondary treated wastewater, river water, and three standard NOM surrogates) were used to elucidate the inhibition mechanisms during photocatalytic degradation of carbamazepine (a model OMP) using TiO_2 and its composites with carbon nanotubes (CNT-TiO_2) under UVC and solar-light irradiation. The results indicated that terrestrially derived NOM with high aromaticity, a low oxygen/carbon atom ratio, and large molecular weight is the major fraction that participates in ROS scavenging, competitive adsorption, and inner filter effect. Furthermore, the modeling analysis suggested that inner filter effect due to NOM and ROS scavenging was the most influential inhibitory mechanism. In the case of secondary treated wastewater, the presence of high concentrations of inorganic species (e.g., PO_4^{3-}, Cl^-, and NO_3^-) together with NOM significantly reduced the photocatalytic degradation of carbamazepine. Overall, the methods and the results of this study provide a comprehensive understanding of the effects of NOM fractions on photocatalysis and highlight the need to further consider the interplay between NOM and background inorganic constituents in photocatalytic degradation of OMP.

1. Introduction

At suitable wavelengths (i.e., $\lambda < 380$ nm), titanium dioxide (TiO_2) facilitates the photocatalytic degradation of various organic micropollutants (OMPs) in aqueous solutions through oxidation processes (i.e., the formation of hydroxyl radicals ($^{\bullet}OH$) and superoxide radicals ($^{\bullet}O_2^-$)) (Arlos et al., 2016; Cai and Hu, 2017; Doong et al., 2001; Haroune et al., 2014; Jallouli et al., 2018). In addition, modifications of TiO_2 by the addition of supporting carbonaceous materials (e.g., activated carbon, graphene and carbon nanotube (CNT)) have been shown to increase the photodegradation rate of different pharmaceuticals and personal care products, pesticides, and synthetic dyes due to high conductivity and modification of the band gap energy (Awfa et al., 2019, 2018; Koli et al., 2016; Miranda et al., 2014; Yao et al., 2008; Yuan et al., 2016; Zouzelka et al., 2016). Moreover, among various carbonaceous materials, CNT showed to be the most promising supporting material due to high mechanical strength, high thermal stability, and potential use of inherently magnetic property for recovery from the solution (Apul et al., 2013; Apul and Karanfil, 2015; Ateia et al., 2017b; Ersan et al., 2017). Also, natural organic matter (NOM) such as humic substances is ubiquitous in natural and engineered waters and influences the performance of photocatalysts for the removal of OMPs. For instance,

* Corresponding author.
** Corresponding author. Department of Civil and Environmental Engineering, School of Environment and Society, Tokyo Institute of Technology, 2-12-1, M1-4, Ookayama, Meguro-ku, Tokyo, 152-8552, Japan.
E-mail addresses: awfadion@gmail.com (D. Awfa), ateia@northwestern.edu (M. Ateia).

https://doi.org/10.1016/j.watres.2020.115643
0043-1354/

low NOM concentrations (i.e., <0.5 mg-C L^{-1}) in water showed enhancement of the photodegradation rate of carbamazepine by creating attraction sites on the TiO_2 particles; however, adverse effects at higher NOM concentrations (i.e., >0.5 mg-C L^{-1}) were observed (Brame et al., 2015; Drosos et al., 2015; Li and Hu, 2018; Ren et al., 2018; Ye et al., 2019; Yuan et al., 2018). These studies indicated the importance of inhibition mechanisms by NOM for the removal of OMPs in water and/or wastewater from treatment plants, where the typical organic concentrations in the water supply and wastewater are more than 0.5 mg-C L^{-1} (Ahmadi et al., 2016; Raeke et al., 2017). Previous studies have reported that NOM interferes with photocatalytic degradation via inner filter effect, radical scavenging, and competition between NOM and target OMPs over the active sorption sites. First, the presence of NOM in water acts as an inner filter which would decrease the availability of light (i.e., energy) to produce reactive oxygen species (ROS) (Ye et al., 2019). Second, in the context of photodegradation, the NOM can reduce the interaction of targeted contaminants close to the catalysts active site (i.e., competitive adsorption) (Ren et al., 2018). Third, the NOM can react with the ROS due to the non-selective nature of the ROS and reduce the effectiveness of the ROS in the photodegradation process (Michael-Kordatou et al., 2015). Among those inhibition mechanisms, Brame et al. (2015) stated that ROS scavenging and competitive adsorption by NOM were the most influential inhibitory mechanisms in a TiO_2 slurry system.

Yet, our understanding of the effect of NOM fractions and their compositions on the photocatalytic degradation of OMP is still fragmentary. The limited observations in previous studies (Table S1) are due to a number of critical factors: 1) most of the studies used high OMP concentrations up to 10 mg/L, which are atypical of environmental concentrations; 2) these studies are not necessarily comparable because only a few NOM types were tested and there were differences in experimental conditions; 3) most of the previous studies focused on the bulk properties of the background NOM (i.e., dissolved organic carbon [DOC]) during the OMP photocatalysis; 4) the light source varied among studies (i.e., UVC and solar irradiation); 5) almost all of the studies focused on TiO_2 as a photocatalyst and no studies examined the effect of NOM on the photocatalysis of OMP by carbonaceous composites of TiO_2; and 6) the studies used only NOM surrogates despite the greater accuracy assessing the inhibition mechanism of NOM in real water samples. Therefore, there is still a need for improved understanding of the photocatalysis of OMP by TiO_2 and its carbonaceous composites in the presence of NOM to adequately assess the potential engineering applications.

Herein, we considered such limitations in the literature and designed this study to elucidate the effects of NOM on the photocatalytic degradation of OMP using TiO_2 and CNT-TiO_2. CNT-TiO_2 was chosen as one modified form of carbonaceous-TiO_2 catalysts that attracted a lot of attention for environmental application, while TiO_2 was used as a benchmark photocatalyst. To this end, the overall objective was to systematically investigate the photocatalytic behavior of carbamazepine as a selected OMP in the presence of three NOM surrogates (i.e., reverse osmosis isolate NOM, humic acid, and fulvic acid) by performing kinetic experiments and using a set of NOM characterization techniques (i.e., DOC, fluorescence, and UV−vis spectroscopy) to document the characteristics and fate of background NOM during the photocatalysis process (i.e., under UVC and solar irradiation). Furthermore, secondary treated wastewater and river water were used to accurately assessed the inhibition mechanism of NOM in real water samples. The specific objectives of research were: 1) to reveal the relationship between the NOM properties and the photocatalytic degradation rate of carbamazepine, 2) to reveal the role of NOM in the inhibition mechanisms, and 3) To determine the relative importance of the inhibition mechanisms (i.e., ROS scavenging, inner filter effect, and competitive adsorption) in CNT-TiO_2 systems based on inhibition model analysis and comparison to TiO_2 system. We focused on the degradation of carbamazepine (an antiepileptic drug) which is persistent, stable against biological processes, direct photolysis, and $^3NOM^{\bullet}$ oxidation (Yan et al., 2017), widely detected in the aquatic environment (Anumol et al., 2016; Sousa et al., 2018; Zhang et al., 2018b), and causes serious toxicity to aquatic organisms (e.g., bacteria, algae, invertebrates, and fish) (Ferrari et al., 2003) and chicken embryos (Kohl et al., 2019). Carbamazepine is also a suitable anthropogenic indicator marker for assessing the efficiency of water or wastewater treatment for the removal of OMPs (Dickenson et al., 2011, 2009).

2. Materials and methods

2.1. Materials

Carbamazepine (≥98%, molecular formula $C_{15}H_{12}N_2O$, molecular weight 236.269 g mol^{-1}), Aeroxide P25 TiO_2 (≥99.5%, Brunauer-Emmet-Teller (BET) specific surface area 35−65 m^2 g^{-1}, average particle size < 21 nm) and high-performance liquid chromatography (HPLC) grade methanol (≥99.8%) were purchased from Sigma-Aldrich Japan (Japan). Industrial grade multi-walled CNT (>90%, diameter 10−20 nm, length 10−30 μm, BET specific surface area 201 m^2 g^{-1}) was obtained from Chengdu Alpha Nano Technology (China). A permanent Nd-Fe-B magnet was purchased from Magna Co. (Japan). Ethanol, HCl, and NaOH were sourced from Kanto Chemical (Japan). Sodium oxalate and isopropanol were purchased from Fujifilm Wako Pure Chemical Industries (Japan). Suwannee River reverse-osmosis isolates (SRNOM), Suwannee River humic acid (SRHA), and Suwannee River fulvic acid (SRFA) were purchased from the International Humic Substances Society (IHSS; USA). The chemical properties of the NOM samples are shown in Table S2. All reagents were of analytical grade and were used as received.

A stock solution of 10 mg L^{-1} carbamazepine was prepared in ultrapure water (18.2 MΩ cm^{-1}). The NOM samples were dissolved in 0.01 M NaOH solution to prepare a 10 g L^{-1} NOM stock solution, and then the pH was adjusted to 7.0 ± 0.2 using 0.1−1 M HCl solutions. The volumes of acid and alkali solutions were recorded and considered when calculating the final NOM concentration. All stock solutions were stored at 4 °C in the dark when not in use, and the desired concentrations were obtained by diluting the stock solutions with ultrapure water. A secondary-treated wastewater (SWW) sample was collected in February 2019 after secondary treatment (activated sludge and secondary clarifier) at a municipal wastewater treatment plant in Tokyo, Japan. Water from the Tama River (RW) was collected at latitude 35°35′ N. and longitude 139°40' E., about 13 km from the mouth of the river in April 2019. After collection, the SWW and RW were filtered with a 0.45-μm PTFE membrane filter (Omnipore JHWP, 47 mm diameter) and were poured into pre-rinsed amber glass bottles (3 L) and stored in a refrigerator (4 °C). The water quality characteristics of the RW and SWW are summarized in Table S3. The pH of the water samples was adjusted to 7.0 ± 0.2 under temperature-controlled laboratory conditions prior to performing the photocatalysis experiments.

2.2. Photocatalytic degradation experiments

In this study, TiO_2 and CNT-TiO_2 composites were used as the catalysts. The detailed preparation and characterization of all catalysts are described in Section S1 in the supporting information. Photocatalytic degradation experiments were conducted in 100 mL

aqueous solution in a 200 mL glass beaker. A magnetic stirrer was used to ensure homogeneous mixing of the catalysts in the solutions. Solutions were prepared having initial concentrations of 500 μg L^{-1} for carbamazepine and 3 mg-C L^{-1} for dissolved organic carbon as either SRNOM, SRFA, or SRHA. The concentrations of carbamazepine and the DOC values of the NOM were determined based on reported average concentrations in the surface water and in the secondary treated domestic wastewater (Carbonaro et al., 2013; Cardoso et al., 2014; Raeke et al., 2017). The pH values of the solutions were adjusted to 7.0 ± 0.2 with 0.01 M HCl and NaOH. The concentration of TiO_2 and CNT-TiO_2 was 0.1 g L^{-1}. The water temperature was kept constant at room temperature (26 ± 3 °C). An 8W UVC lamp (GLK8MQ; Sankyo Denki, Japan) was installed to provide ultraviolet radiation with λ = 254 nm and light intensity 80 W m^{-2}. In the case of solar irradiation, a solar simulator (MS-35AAA; Ushio Lighting Edge Technologies, Japan) with light intensity of 1000 W m^{-2} was used as a light source (Lee et al., 2017b). For all experiments, prior to irradiation, the suspension was stirred in the dark for 60 min to allow an adsorption equilibrium of carbamazepine to be established on the catalyst surface. It was confirmed that additional stirring for 120 min resulted in no further adsorption of carbamazepine. During irradiation, an aliquot (50 mL) of slurry was withdrawn after 5, 10, 15, 20, and 30 min, respectively. Blank experiments in ultrapure water and also without catalysts were conducted to test the photocatalysis in the absence of NOM and photolysis. All the experiments were performed in duplicate. Moreover, to elucidate the main oxidizing agents produced by the CNT-TiO_2 system, isopropanol (•OH quencher) and sodium oxalate (h^+ quencher) were employed in the photocatalysis process (i.e., in ultrapure water) (Zhang et al., 2018a).

The effect of water matrices was evaluated by spiking carbamazepine into SWW and RW (500 μg L^{-1}), followed by photocatalytic degradation using CNT-TiO_2 under UVC irradiation (One 8W UVC lamp, λmax = 254 nm, light intensity 80 W m^{-2}, GLK8MQ; Sankyo Denki). UVC was used as the source of the light irradiation due to the higher energy (i.e., higher photocatalytic activity). As a control experiment, 500 μg L^{-1} of carbamazepine was also spiked into the SRNOM and compared alongside the SWW and RW. The SRNOM was selected because its NOM property is similar to that of the SWW and the RW in terms of fluorescence index [FI] values, and a UVC lamp was used as an irradiation source, considering the high energy of this source which would favor the production of radicals. The experiments were performed under the same operating conditions examined for ultrapure water spiked with NOM standards (i.e., SRNOM, SRFA, and SRHA). The detailed analytical procedures (i.e., HPLC, LC-MS/MS, IC, TOC, UV, and fluorescence) are described in Section S2. The photocatalytic activity of the TiO_2 and CNT-TiO_2 are described using a pseudo-first-order kinetic equation Eq. (1) (Ateia et al., 2020):

$$\ln\frac{Ct}{Co} = -k.t \tag{1}$$

where Co and Ct are the initial concentration and concentration of the carbamazepine at a certain time, respectively, k is the pseudo-first-order rate constant (min^{-1}), and t is the time (min).

2.3. Model application

The NOM inhibition model (Brame et al., 2015) (Eqs. (2)–(7)) for photocatalytic degradation was applied to elucidate the NOM inhibition mechanism (i.e., ROS scavenging, competitive adsorption, and inner filter effect) in the experiment. The results from photocatalytic degradation of carbamazepine under solar irradiation in the presence of the SRNOM were chosen due to the availability of relevant parameters in the literature and the similar NOM characteristics to SWW and RW.

$$\frac{dC_A}{dt}\text{non} = -k_A C_A C_{ROS,S}\left(\frac{1}{1+\frac{k_A C_A}{D}} + \frac{K_A}{1+K_A C_A}\right) \tag{2}$$

$$C_{ROS,B} = \frac{C_{ROS,S}}{1+\frac{k_A C_A}{D}} \tag{3}$$

$$P_{ROS,0} = k_A C_{ROS,B} C_A - \frac{k_A C_{ROS,S} K_A C_A}{1+K_A C_A} \tag{4}$$

$$\frac{dC_A}{dt}\text{inhibit} = \frac{-P_{ROS,0}}{1+\frac{k_N C_N (F+K_N S)}{k_A C_A (F+K_A S)}} 10^{-\mu L C_N} \tag{5}$$

$$F = \frac{1}{1+\frac{k_A C_A + k_N C_N}{D}} \tag{6}$$

$$S = \frac{1}{1+K_A C_A + K_N C_N} \tag{7}$$

Here, dC_A/dt non is the degradation rate of carbamazepine in the absence of the SRNOM, dC_A/dt inhibit is the degradation rate of carbamazepine in the presence of the SRNOM, k_A is the reaction rate constant of carbamazepine, k_N is the reaction rate constant of carbamazepine, K_A is the Langmuir adsorption constant of carbamazepine, K_N is the Langmuir adsorption constant of SRNOM, D is the diffusion coefficient, $C_{ROS,B}$ is the concentration of ROS in the bulk solution, $C_{ROS,S}$ is the concentration of the ROS on the surface of the catalyst, $P_{ROS,0}$ is the production of ROS in the absence of the SRNOM, P_{ROS} is the production of ROS in the presence of the SRNOM, C_A is the equilibrium concentration of carbamazepine, C_N is the equilibrium concentration of the SRNOM, and μL is inner filter constant. Modeling parameters are given in Table S4. The reaction rate constants (k_A and k_N) for •OH and the diffusion constant (D) for •OH were taken from the literature. The Langmuir adsorption constants (K_A and K_N) were taken from the literature sources for identical CNTs and modified accordingly with the specific surface area for the CNT-TiO_2 used in this work. The degradation rate for carbamazepine removal in the absence and presence of NOM (dC_A/dt non and dC_A/dt inhibit, respectively), C_A, and C_N were measured from the experiments (some data were used for validation). The production of ROS in the absence of NOM ($P_{ROS,0}$) and inner filter constant (μL) were calculated using Eqs. (2)–(7). After acquiring all the parameters, prediction of the degradation removal rate of carbamazepine in the presence of NOM (dC_A/dt inhibit model) was performed and the results compared with the dC_A/dt inhibit values from experiments (dC_A/dt inhibit exp.) to validate the model; this was followed by calculation of the root mean square error (RMSE). Nonlinear regression by Microsoft Excel Solver was used to adjust the constants (i.e., k_A, k_N, K_A, K_N, D, $P_{ros,0}$, and μL). Furthermore, point elasticity analysis was performed to check the most influential mechanism for NOM inhibition (Brame et al., 2015). The point of elasticity is defined as the percent change in the dependent variable (i.e., carbamazepine degradation rate) divided by the percent change in an independent variable. The K_A/K_N, k_A/k_N, and μL parameters are the major independent variables in the inhibition model, which can describe the competitive adsorption, ROS scavenging, and inner filter effect, respectively (Brame et al., 2015).

3. Results and discussion

3.1. Material characterization

The morphology of the CNT-TiO_2 revealed that TiO_2 clusters were attached on the surface of the CNT (SEM image, Fig. S1), which was further confirmed by TEM-EDX analysis (Figs. S2 and S3). The surface area, the total pore volume, and the pore distribution of the samples are listed in Table 1. The specific surface area of the CNT-TiO_2 was three times higher than that of the TiO_2. Furthermore, the CNT-TiO_2 showed a narrower bandgap in visible light region (2.8 eV ≈ 440 nm) than that of the TiO_2 (3.3 eV ≈ 376 nm) (Fig. S4), which suggested that CNT-TiO_2 may function as a superior photocatalytic material and may be active under both solar and UV irradiation. The crystalline property of TiO_2 and the prepared CNT-TiO_2 was confirmed by XRD analysis (Fig. S5). The diffraction peak of TiO_2 consisted of anatase (main diffraction peak at 2θ ≈ 25.3°) and rutile (main diffraction peak at 2θ ≈ 27.4°) TiO_2 peaks. The CNT-TiO_2 had four main diffraction peaks at 2θ ≈ 26° and 43°, which were attributed to the CNT graphite-like structure, and at 2θ ≈ 25.3° and 27.4°, which were attributed to anatase and rutile TiO_2 peaks, respectively. More details on the characterization of the CNT-TiO_2 are available in a previous report (Awfa et al., 2019).

3.2. Photolysis and photocatalytic degradation of carbamazepine

Photolysis of carbamazepine by UVC and solar irradiation was well fitted by the pseudo-first-order kinetic model (Fig. S6). Direct photolysis of carbamazepine under UVC and solar irradiation showed very low removal (<5%), with photolysis rate constants ($k_{carbamazepine}$) of 5 ± 1 × 10^{-4} min^{-1} and 4 ± 0.7 × 10^{-4} min^{-1} during UVC and solar irradiation, respectively. The amide bonds in carbamazepine make it highly resistant to UVC (Deng et al., 2013). In the case of direct photolysis under solar irradiation, carbamazepine does not have functional groups that absorb radiation >290 nm (i.e., corresponding to the main solar irradiation spectrum) (Wang et al., 2017). During photocatalysis, carbamazepine was rapidly degraded with $k_{carbamazepine}$ values of 4.75 ± 0.07 × 10^{-2} min^{-1} (UVC/TiO_2), 7.0 ± 0.08 × 10^{-2} min^{-1} (UVC/CNT-TiO_2), 3.95 ± 0.07 × 10^{-2} min^{-1} (solar/TiO_2), and 5.5 ± 0.06 × 10^{-2} min^{-1} (solar/CNT-TiO_2), as shown in Fig. 1. Given that direct photolysis was negligible, it is evident that the removal of carbamazepine was due mainly to its reaction with radicals produced by photocatalysis. The participation of radicals in carbamazepine photocatalytic degradation was then clarified by the addition of isopropanol (IP) as a scavenger for •OH and sodium oxalate (SO) as a scavenger of h^+. As shown in Fig. 1, the addition of IP and SO resulted in the inhibition of carbamazepine photocatalytic degradation, suggesting that both •OH and h^+ participated in the photocatalysis of carbamazepine by TiO_2 and CNT-TiO_2. In general, the photocatalytic activity (i.e., k) of CNT-TiO_2 was higher than TiO_2 because 1) the excited CNT can inject electrons into TiO_2 which increases the photocurrent (Woan et al., 2009), 2) the excitation electron from CNT can combine with dissolved O_2 to form superoxide (Woan et al., 2009), and 3) CNT provides suitable sites for the sorption of contaminants, which act as an electron sink and facilitates visible light absorption due to the Ti—O—C linkage (i.e., bandgap reduction) (Awfa et al., 2019). Furthermore, UVC photocatalysis showed higher $k_{carbamazepine}$ values than solar irradiation because the shorter wavelength (i.e., UVC) is associated with a greater photon energy that can promote electrons to the conduction band with high kinetic energy (Phong and Hur, 2016).

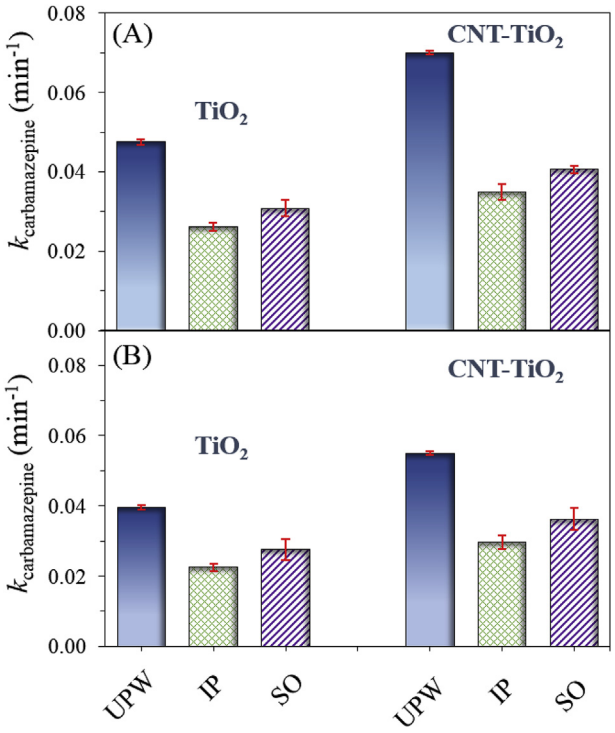

Fig. 1. Photocatalysis rate constant of carbamazepine by UVC irradiation (A) and solar irradiation (B) in ultrapure water (UPW), UPW spiked with isopropanol (IP), and UPW spiked with sodium oxalate (SO). $[Carbamazepine]_o$ = 500 μg L^{-1}, [IP] = 2 mM, [SO] = 2 mM. Data and error bars indicate the average and standard error from duplicate experiments.

3.3. Photolysis and photocatalytic degradation of carbamazepine in the presence of different NOM surrogates

The NOM inhibition mechanisms: The addition of three different NOM surrogates inhibited the carbamazepine photolysis under UVC and solar irradiation (Fig. 2). These inhibitions of carbamazepine photolysis were due presumably to inner filter effect of the SRNOM, the SRFA, and the SRHA (Lee et al., 2014). Both the SRFA and the SRHA with higher aromatic content (i.e., high $SUVA_{254}$ value) exhibited more inhibition than the SRNOM for the photolysis of carbamazepine. Apparently, the NOM with high aromatic content can intercept the light transmission and also increase the energy consumption from UVC and solar irradiation (Guerard et al., 2009).

Furthermore, the inhibitory effect of NOM on photocatalysis may also be due to the surface deactivation of TiO_2 and CNT-TiO_2 by

Table 1
Characteristics of TiO_2 and CNT-TiO_2 used in this study.

Catalysts	Carbon contents (%)	SA (m^2 g^{-1})	PVtotal (cm^3 g^{-1}) [%]	PVmicro (cm^3 g^{-1}) [%]	PVmeso (cm^3 g^{-1}) [%]	PVmacro (cm^3 g^{-1}) [%]
TiO_2	–	56	0.24 [100]	0.002 [0.8]	0.13 [53.7]	0.11 [45.4]
CNT-TiO_2	32	151	1.2 [100]	0.01 [0.8]	0.65 [54.4]	0.54 [44.8]

SA: surface area; PVtotal: total pore volume; PVmicro: volume of micropores (PV < 2 nm); PVmeso: volume of mesopores (2 < PV 50 nm); and PVmacro: volume of macropores (PV > 50 nm).

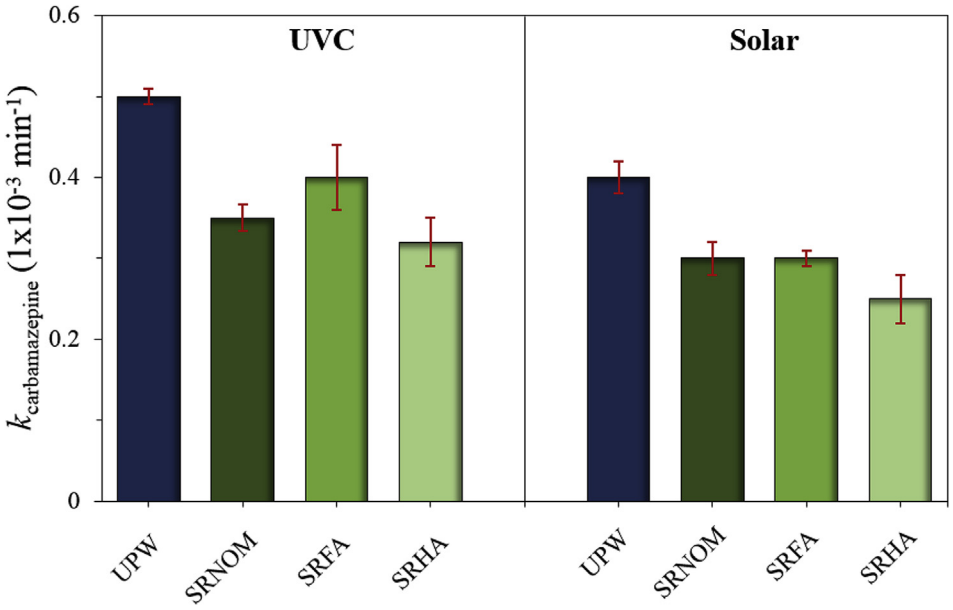

Fig. 2. Photolysis rate constants of carbamazepine by UVC and solar irradiation in ultrapure water (UPW) and in the presence of different NOM surrogates. $[Carbamazepine]_o$ = 500 μg L^{-1} and [SRNOM] = [SRFA] = [SRHA] = 3 mg C L^{-1}. Data and error bars indicate the average and standard error from duplicate experiments.

adsorption and/or radical scavenging (Brame et al., 2015). The adsorbed NOM was capable of reducing the interaction of carbamazepine close to the catalyst active sites for the photodegradation process (i.e., competitive adsorption) and NOM can also scavenge the holes (h^+) in the catalyst valence band (Ren et al., 2018). As indicated in Fig. S7, the competitive adsorption of NOM reduced the adsorption capacity of carbamazepine onto CNT-TiO_2 in the order SRHA > SRFA > SRNOM. The difference in this competitive adsorption can be attributed to the higher aromaticity of the SRHA, as indicated by the $SUVA_{254}$ value (Ateia et al., 2017a). The presence of the CNT provided a high surface area with hydrophobic sites in the CNT-TiO_2 composite. However, in the case of TiO_2 alone, the presence of NOM had a minimal effect on the adsorption of carbamazepine on TiO_2, implying that there was no competitive adsorption between carbamazepine and NOM. This is apparently due to the surface hydrophilicity and limited surface area of TiO_2 (Yang and Xing, 2009; Yuan et al., 2018). Thus, the inhibitory effect of NOM was attributed mainly to inner filter effect and the radical scavenging for TiO_2. However, in the case of CNT-TiO_2, competitive adsorption together with inner filter effect and radical scavenging were responsible for the mechanism of NOM inhibition in photocatalytic degradation of carbamazepine.

The role of NOM composition: The addition of the NOM surrogates negatively affected the photocatalytic degradation of carbamazepine by TiO_2 and CNT-TiO_2 under UVC and solar irradiation (Fig. 3 and Fig. S8), which is consistent with previous studies (Doll and Frimmel, 2005; Haroune et al., 2014). The degree of inhibition of carbamazepine photocatalysis by different NOM surrogates followed the order SRHA > SRFA > SRNOM, implying the dependence of the carbamazepine photocatalysis degradation rate on the NOM characteristics. NOM interferes with the photocatalytic mechanisms via inner filter effect, radical scavenging, and adsorbed NOM competes for active sites with the targeted OMP. Despite the lower photodegradation rate in the presence of NOM, the reduction in the photodegradation rate of CNT-TiO_2 (i.e., ~50%–80% inhibition) was less than that of TiO_2 (i.e., ~55%–90%) for both UVC and solar irradiation perhaps due to the fact that the high surface area of the composite provided sufficient active sites for the photocatalytic degradation on CNT-TiO_2 in contrast to that for TiO_2 (Awfa et al., 2019). The changes in DOC during photocatalytic degradation are described in Section S3 in the supporting information.

In addition, five excitation emission matrix (EEM) peaks having different excitation/emission pairs were investigated to understand the effects of several NOM fractions with different sources and relative size variations on the photocatalytic degradation of

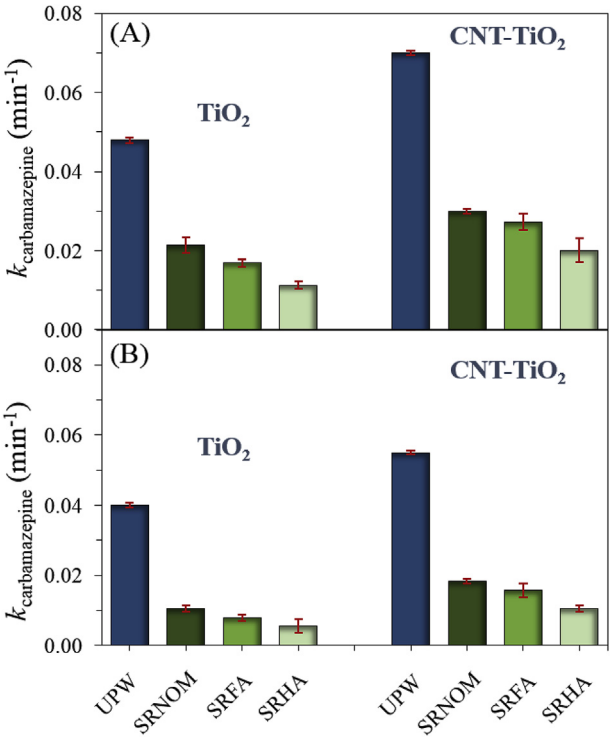

Fig. 3. Photocatalysis rate constants of carbamazepine by UVC irradiation (A) and solar irradiation (B) in the presence of different NOM surrogates. $[Carbamazepine]_0$ = 500 μg L^{-1} and [SRNOM] = [SRFA] = [SRHA] = 3 mg-C L^{-1}. Data and error bars indicate the average and standard error from duplicate experiments.

carbamazepine (Table 2). Adsorption of NOM peaks onto TiO_2 and CNT-TiO_2 were in the order peak C > M > A > T > B (Fig. S9). This order can be explained by the linkage of the terrestrial humic-like component with larger and more hydrophobic NOM fractions, which typically have a higher adsorption affinity on the catalysts (Zhao et al., 2018). Irrespective of the NOM fractions, the adsorption onto CNT-TiO_2 was higher than onto TiO_2 because CNT-TiO_2 is hydrophobic and has a higher specific surface area. In the case of photolysis (Fig. S10), the highest photolysis degradation of the NOM fraction was peak T with an excitation wavelength at 275 nm under UVC irradiation (UVC irradiation λmax = 254 nm). In contrast, the NOM fraction degradation under solar irradiation (solar irradiation λmax = 550 nm) was in the order C > M ≈ A > T > B. These results were consistent with previous photolysis studies using UVC irradiation (Phong and Hur, 2016) and solar irradiation (Moran et al., 2000). The highest removal of NOM fractions was found when the excitation peak wavelengths were close to the maximum irradiation wavelength, followed by those with longer to shorter peak excitation wavelengths (Del Vecchio and Blough, 2002). For photocatalytic degradation, the order of the NOM photocatalytic degradation rate (k_{NOM}) was peak C > M > A > T > B for both TiO_2 and CNT-TiO_2 under UVC and solar irradiation (Fig. 4). A previous study indicated that the different degradation behaviors of the NOM peaks can be explained by the catalyst-associated reaction pathways (Phong and Hur, 2015). The NOM peak that was adsorbed or adhered to the catalyst's surface was likely to be more preferably degraded by hydroxyl radicals and/or react with holes (h^+), leading to the highest degradation. Therefore, it was presumed that peak C gives the highest $k_{carbamazepine}$ inhibition in carbamazepine photocatalytic degradation.

Previous studies reported that the fluorescence index (FI) can be a superior indicator for investigation of the changes of NOM during several water treatment processes such as photocatalysis (Bekbolet and Sen-Kavurmaci, 2015), photocatalytic disinfection (Birben et al., 2017), ozonation (Rodríguez et al., 2014), and adsorption (Ateia et al., 2017a). In this study, the FI values were calculated to evaluate the preferential removal of NOM fractions during carbamazepine photocatalytic degradation. As shown in Table S2, the FI values for the samples (i.e., before photocatalysis) indicated that the SRHA and the SRFA were more likely to be terrestrial-derived NOM (FI < 1.2). However, the SRNOM shared the characteristics of both terrestrial and microbial aquatic NOM (1.2 < FI < 1.8). As illustrated in Fig. 5, the FI values of all NOM samples increased after photocatalysis under UVC and solar irradiation (FI > 1.2). This indicated the preferential photocatalytic degradation of terrestrially derived compounds. Previous studies tested the same standard NOM samples, reporting that terrestrially derived NOM is rich in aromatic moieties (Ateia et al., 2017a) and has a high average molecular weight (Shimabuku et al., 2017). FI is related to the source of NOM. Thus, the increase of the FI values further suggests that terrestrially derived NOM (i.e., NOM fractions with high molecular weight and high aromatic moieties) were preferentially removed during the photocatalytic degradation.

Further analysis of the results indicated that $k_{carbamazepine}$ had correlations with the O/C ratio, $SUVA_{254}$ and FI, and the degradation rate of Peak C (Fig. 6). Also, NOM with lower O/C ratios tended to have a higher inhibition in carbamazepine photocatalytic degradation (Fig. 6A). Lower O/C ratios implied the NOM contained fewer oxygenic groups, especially carbonyl and/or carboxylic groups. A similar trend was previously observed for the preferential degradation of NOM with low O/C ratio by TiO_2 (Lv et al., 2017). In addition, terrestrially derived NOM (low FI value) with high aromaticity (high $SUVA_{254}$ value) exhibited higher inhibition of $k_{carbamazepine}$ (Fig. 6B and C), which is in agreement with Fig. 6D, where higher degradation rates for Peak C (terrestrial humic-like and high molecular weight components of NOM) led to a decrease in $k_{carbamazepine}$.

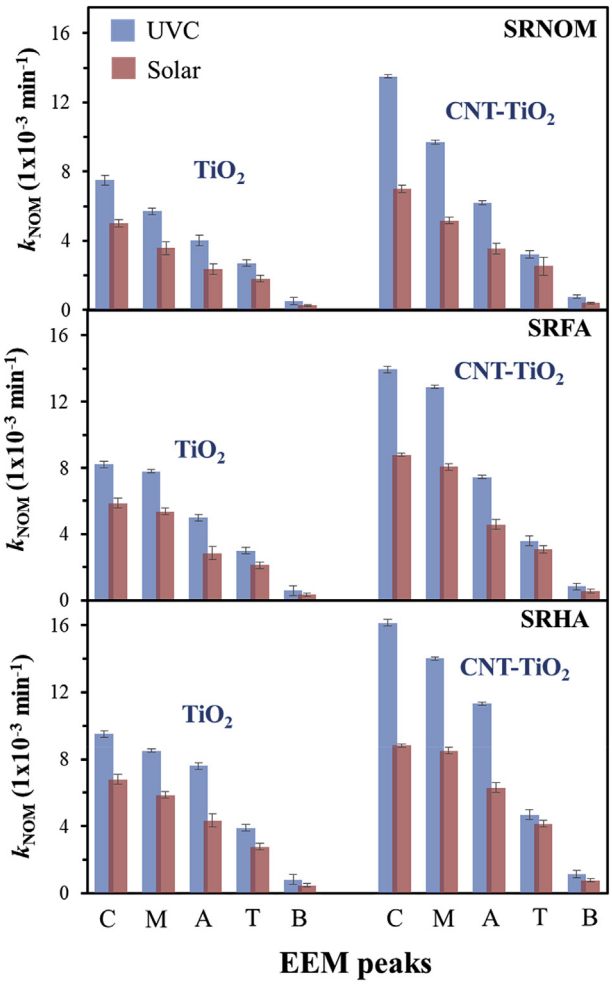

Fig. 4. Photocatalysis rate constants of NOM for different peaks. $[Carbamazepine]_o$ = 500 μg L^{-1} and [SRNOM] = [SRFA] = [SRHA] = 3 mg-C L^{-1}. Data and error bars indicate the average and standard error from duplicate experiments.

Table 2
The excitation-emission pairs (peak picking) used in this study.

Peak	Excitation (nm)	Emission (nm)	Peak description [a]
B	275	306	Protein-like component which resembles tyrosine but may be free or combined amino acid
T	275	340	Protein-like component which resembles tryptophan but may be free or combined amino acid
A	240	444	Terrestrial humic-like component and may consist of low molecular weight compounds
M	300	444	Marine humic-like component and may consist of intermediate molecular weight compounds
C	350	460	Terrestrial humic-like component and may consist of high molecular weight compounds

[a] References (Coble, 1996; Lee et al., 2017a).

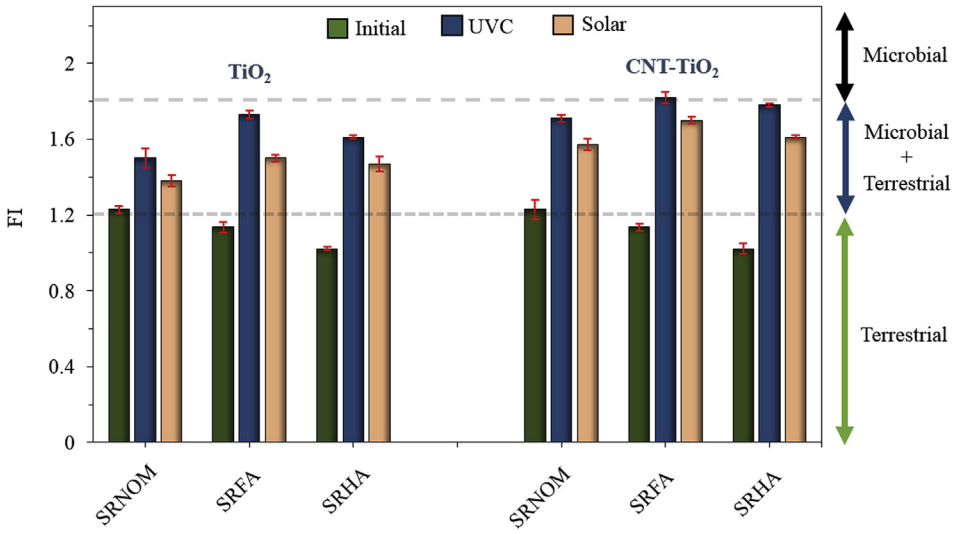

Fig. 5. Changes in the fluorescence index (FI) for all NOM samples in this study. $[Carbamazepine]_o$ = 500 μg L^{-1} and [SRNOM] = [SRFA] = [SRHA] = 3 mg-C L^{-1}. Data and error bars indicate the average and standard error from duplicate experiments.

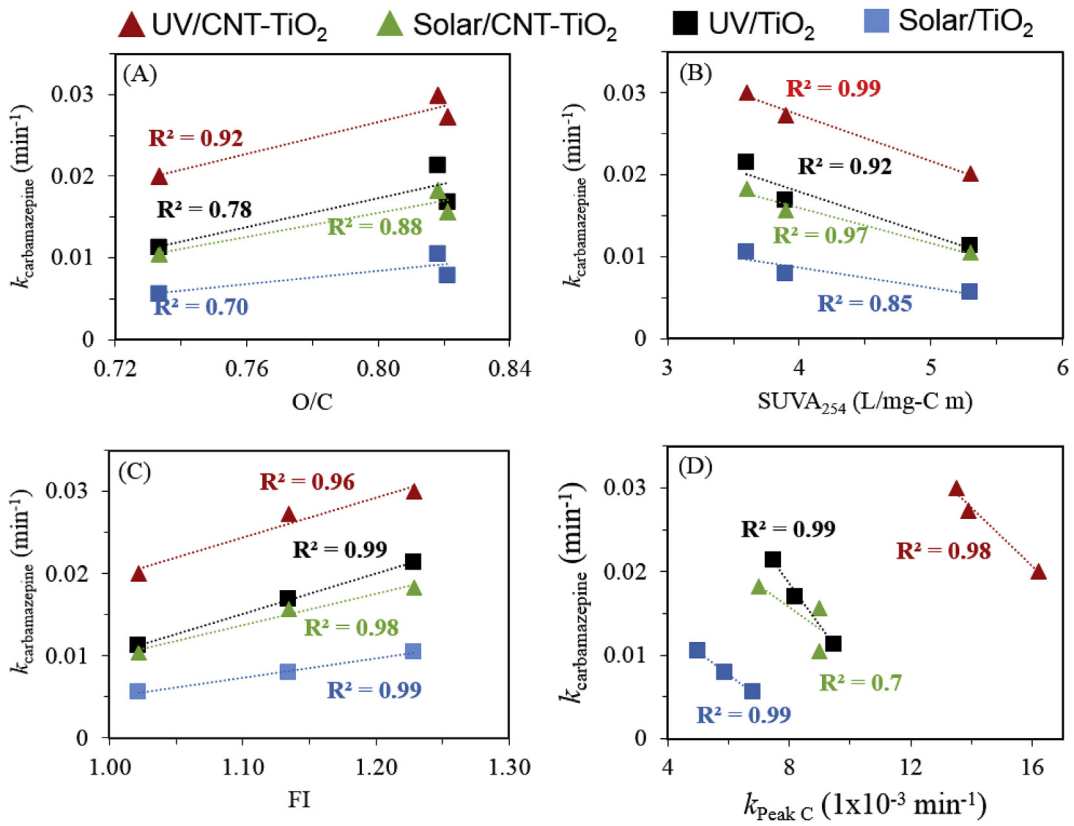

Fig. 6. Relationships of photocatalytic degradation rate constants (k) of carbamazepine to (A) O/C atomic ratio, (B) $SUVA_{254}$, (C) Fluorescence index (FI) and (D) degradation rate of peak C ($k_{Peak\ C}$).

3.4. The relative importance of each inhibition mechanism in the photocatalytic degradation

The previous study indicated that the inhibition model gave a reasonable prediction (R^2 > 0.88) for the photocatalytic degradation of the OMP in the presence of background NOM with TiO_2 under UVA irradiation, and the relative importance of NOM inhibition followed the order ROS scavenging > competitive adsorption > inner filter effect (Brame et al., 2015). Therefore, the existing inhibition model could also be useful for explaining the role of each NOM inhibition mechanism in the photocatalytic degradation of carbamazepine using CNT-TiO_2. In this study, the model predicted the degradation rates of carbamazepine using CNT-TiO_2 with a high degree of accuracy (R^2 > 0.8, RMSE = 0.0005 mg L^{-1} min^{-1}, Fig. S11). This result validated the existing NOM inhibition model and showed its capability to predict

degradation of OMPs in water containing NOM using CNT-TiO_2 under solar light irradiation. As shown in Fig. 7, the relative importance of the NOM inhibition mechanism in CNT-TiO_2 photocatalysis followed the order ROS scavenging > inner filter effect > competitive adsorption. This finding was contrary to the previous study conducted by Brame et al., (2015), where competitive adsorption was found to be relatively more important than inner filter effect in the case of TiO_2. This inhibitory effect depends significantly on the physicochemical properties of the target compound, the catalyst, and the quality and quantity of NOM. Despite the fact that a similar NOM (i.e., SRNOM) was used, it should be noted that the previous study involved TiO_2 while in this study, CNT-TiO_2 was used as the photocatalyst. The high surface area of the CNT-TiO_2, unlike TiO_2, provided sufficient active sites for the adsorption. Therefore, the difference in the catalyst properties affected the relative order of inner filter effect and competitive adsorption. Yet, the role played by NOM as a ROS scavenging still provided the most important inhibition mechanism in the photocatalytic degradation of OMP for both TiO_2 and CNT-TiO_2. Furthermore, a change of NOM property would also affect the CNT-TiO_2 photocatalysis. In the case of NOM with higher aromaticity and molecular weight, there would be an increase in the values of K_N (i.e., decrement of K_A/K_N), k_N (i.e., decrement of k_A/k_N), and μL, which would equate to a larger influence of the inhibitory compound and therefore lead to a decrement in the degradation rates. According to the point elasticity values of 0.4, 0.7, and 0.6 for K_A/K_N, k_A/k_N, and μL, a 10% change in competitive adsorption (K_A/K_N), ROS scavenging (k_A/k_N), and inner filter effect (μL) would result in a 4%, 7%, and 6% reduction in the modeled degradation rates, respectively.

3.5. Photocatalytic degradation of carbamazepine in secondary treated wastewater and river water

Further insight into the mechanism of NOM inhibition was gained from studies using SWW and RW. The carbamazepine photodegradation removal obtained in these waters is summarized in Fig. 8. The degree of inhibition of carbamazepine photocatalysis by the different water matrices followed the order SWW > SRNOM 3 mg-C L^{-1} > RW > SRNOM 1 mg-C L^{-1}, and contrary to the previous findings where $SUVA_{254}$ and FI showed a strong linear relationship with carbamazepine removal (Fig. 6B and C). The lowest removal rate was obtained with the secondary wastewater (i.e., the lowest $SUVA_{254}$ and FI value) with the carbamazepine removal being around 40%. However, small reductions in photocatalytic degradation removal (less than 15% after 30 min) were observed with SRNOM (1 mg-C L^{-1} and 3 mg-C L^{-1}) and RW water matrices in comparison to pure water. The highest catalyst deactivation in SWW was possibly attributed to the combined effect of the presence of both the different mineral species and organic matter at relatively high concentration in comparison with other water matrices (Table S3). The predominant inorganic species in the SWW were NO_3^-, PO_4^{3-}, and Cl^-, with the concentrations varying from 22 mg L^{-1} to 76 mg L^{-1}. The presence of high concentrations of inorganic species has been linked to the competition for active sites and free radicals (i.e., ROS scavenging). In addition to these inorganic species, SO_4^{2-} was also detected in RW and SWW (data not shown). Even at low concentrations (<0.01 M), SO_4^{2-}, PO_4^{2-} and Cl^- decreased the photocatalytic degradation rate for targeted contaminants by reacting with h^+ and $^{\bullet}OH$ producing $SO_4^{\bullet}$ radicals, $PO_4^{\bullet}$ radicals and $Cl^{\bullet}$ radicals, respectively (Abdullah, 1990). $SO_4^{\bullet}$ radicals, $PO_4^{\bullet}$ radicals and $Cl^{\bullet}$ radicals are known to be less reactive than $^{\bullet}OH$ radicals. Moreover, SO_4^{2-} can cause stronger deactivation effect than chlorides because SO_4^{2-} scavenges reactive oxygen species at higher rate (Rioja et al., 2016). In the case of NO_3^-, at high concentration, NO_3^- could be absorbed on the catalyst surface and compete for the active sites with the target pollutants (Lado Ribeiro et al., 2019). These phenomenon have been observed for the photocatalytic degradation of clofibric acid in recycled wastewater using UVA-TiO_2 (Rioja et al., 2016).

The FI values for all water samples before photocatalysis indicated that all water samples shared the characteristics of both terrestrial and microbial aquatic NOM (1.2 < FI < 1.8). The preferential photocatalytic degradation of terrestrially derived organic matter during the photocatalytic degradation of carbamazepine in the presence of organic matter in SWW and RW was confirmed (Fig. S12). However, the increase of the FI values for SWW after the treatment was not higher relative to those in RW and SRNOM. One possible reason for this is the higher abundance of microbial-

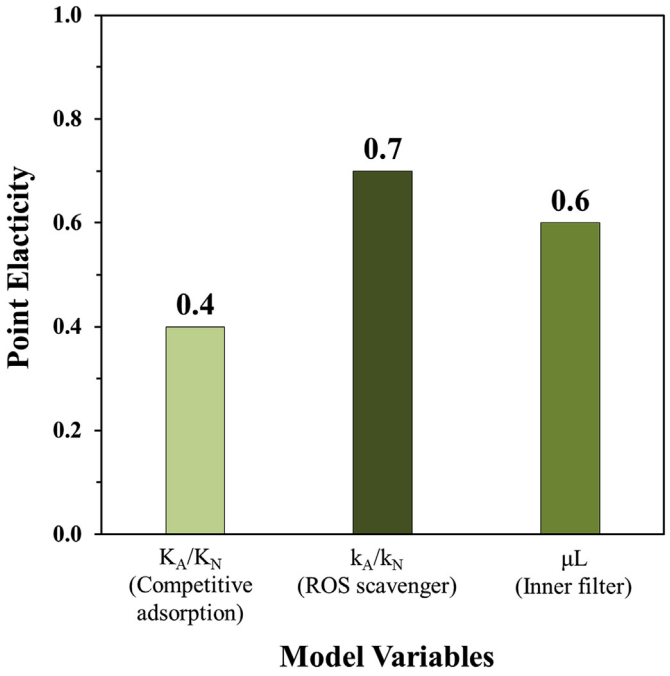

Fig. 7. The relative importance of the NOM inhibition mechanism in CNT-TiO_2 photocatalysis for the removal of carbamazepine under solar irradiation. The tested NOM were SRNOM, SRHA, and SRFA.

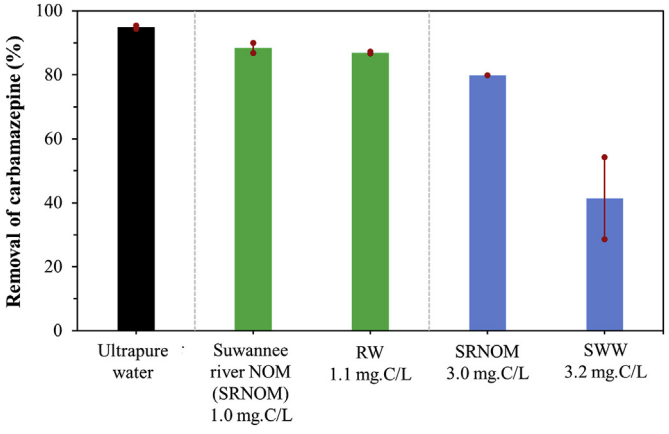

Fig. 8. Photocatalytic degradation of carbamazepine by CNT-TiO_2 under UVC irradiation ($[Carbamazepine]_o$ = 500 μg L^{-1}, irradiation time = 30 min). Data and error bars indicate the average and standard error from duplicate experiments.

derived organic matter (i.e., small molecular weight and low aromaticity) compared with terrestrial-derived organic matter (i.e., large molecular weight and high aromaticity) in the SWW water sample (Carstea et al., 2016), which is less preferentially degraded by photocatalysis (Keen et al., 2014). Further, the EEM peaks indicated that photocatalytic degradation removal of NOM peaks followed the order peak C > M > A > T > B for both SRNOM and RW (Fig. S13), which is in agreement with the previous findings in the presence of NOM surrogates (e.g., SRNOM, SRFA, and SRHA). However, in the case of the SWW, the removal of NOM peaks followed the order peak T > B > M > A > C. This indicates that protein-like and marine-like components were likely to inhibit the CNT-TiO2 photocatalysis in the SWW to a greater extent compared to humic-like components. Although peak T (i.e., microbial derived NOM) has a low adsorption affinity, due to the higher relative abundance of microbial derived NOM in SWW and the non-selective nature of the ROS, the ROS scavenging by peak T (i.e., higher removal of peak T) may have occurred. This finding is in agreement with the calculation of the relative importance of each inhibition mechanism of NOM (i.e., section 3.4), where ROS scavenging was still the most important inhibition mechanism in the CNT-TiO2 photocatalysis. Another possible reason was that UV photocatalysis preferentially degraded the aromatic compounds and phenols in the SWW; because the energy of UV photocatalysis is limited, the unsaturated bonds would have been transformed into carboxylic acids, aldehydes, and more (Meng et al., 2016). Thus, UV photocatalysis would have increased and/or maintained the abundance of fulvic acid-like and humic acid-like compounds in the SWW sample.

The photochemical process of contaminant degradation is energy-intensive and the electrical energy per order (E_{EO}) represents a major fraction of the total operating cost (Vishnuganth et al., 2016). This approach allows for simple comparison and provides data required for scale-up and economic analysis. The E_{EO} values (kWh m^{-3} $order^{-1}$) calculated for carbamazepine removal in ultrapure spiked with NOM, RW, and SWW are shown in Fig. S14. In general, the electrical energy consumption for the photocatalytic degradation of carbamazepine in water containing NOM using CNT-TiO_2 ranged from 43 to 231 kWh m^{-3} $order^{-1}$, and where the median E_{EO} values for UV-TiO_2 photocatalysis was reported as being >100 kWh/m^3/order (Miklos et al., 2018). Therefore, the synergetic effect of CNT-TiO_2 leads to efficient UV photocatalysis (i.e., SRNOM and RW cases) and supports the applicability of photocatalysis in water treatment process.

4. Conclusions

The main target of this study was to elucidate the inhibition mechanisms during photocatalytic degradation of carbamazepine using TiO_2 and CNT-TiO_2 under UVC and solar-light irradiations. The results indicated that terrestrially derived NOM with high aromaticity and large molecular weight is the major fraction of organic matter that participates in the inhibition process. However, in the case of SWW, microbial-derived NOM, which is rich in protein-like compounds, is the major fraction that participates in the inhibition. Further analysis using NOM inhibition model indicated that the relative importance of the NOM inhibition mechanism in CNT-TiO_2 photocatalysis process followed the order ROS scavenging > inner filter effect > competitive adsorption. In addition, the presence of other water reaction chemistries, particularly those involving inorganic species, affected the photocatalysis performance by acting as radical scavengers. Overall, CNT-TiO_2 may exhibit a photodegradation activity and participate in an energy-efficient process for the removal of carbamazepine depending on the nature of the dissolved organic matter property of the system. By providing a comprehensive understanding of the effect of NOM in TiO_2 and CNT-TiO_2 photocatalysis, this study will promote the introduction of new treatment strategies to enhance the applicability the photocatalysis process.

Declaration of competing interest

The authors declare that they have no known competing financial interests or personal relationships that could have appeared to influence the work reported in this paper.

Acknowledgements

The authors would like to acknowledge the Ookayama Materials Analysis Division Technical Department in Tokyo Institute of Technology for SEM, TEM, EDX, and XRD analyses. Dion Awfa is grateful for a scholarship from Indonesia Endowment Fund for Education (LPDP). This work was supported by JSPS KAKENHI (Grant Number 18H01566) and LPDP.

Appendix A. Supplementary data

Supplementary data to this article can be found online at https://doi.org/10.1016/j.watres.2020.115643.

References

Abdullah, M., 1990. Effects of common inorganic anions on rates of photocatalytic oxidation of organic carbon over illuminated titanium dioxide. J. Phys. Chem. 94, 6820–6825. https://doi.org/10.1021/j100380a051.

Ahmadi, M., Ramezani Motlagh, H., Jaafarzadeh, N., Mostoufi, A., Saeedi, R., Barzegar, G., Jorfi, S., 2016. Enhanced photocatalytic degradation of tetracycline and real pharmaceutical wastewater using MWCNT/TiO2 nano-composite. J. Environ. Manag. 186, 55–63. https://doi.org/10.1016/j.jenvman.2016.09.088.

Anumol, T., Vijayanandan, A., Park, M., Philip, L., Snyder, S.A., 2016. Occurrence and fate of emerging trace organic chemicals in wastewater plants in Chennai, India. Environ. Int. 92–93, 33–42. https://doi.org/10.1016/j.envint.2016.03.022.

Apul, O.G., Karanfil, T., 2015. Adsorption of synthetic organic contaminants by carbon nanotubes: a critical review. Water Res. 68, 34–55. https://doi.org/10.1016/j.watres.2014.09.032.

Apul, O.G., Wang, Q., Zhou, Y., Karanfil, T., 2013. Adsorption of aromatic organic contaminants by graphene nanosheets: comparison with carbon nanotubes and activated carbon. Water Res. 47, 1648–1654. https://doi.org/10.1016/j.watres.2012.12.031.

Arlos, M.J., Hatat-Fraile, M.M., Liang, R., Bragg, L.M., Zhou, N.Y., Andrews, S.A., Servos, M.R., 2016. Photocatalytic decomposition of organic micropollutants using immobilized TiO2 having different isoelectric points. Water Res. 101, 351–361. https://doi.org/10.1016/j.watres.2016.05.073.

Ateia, M., Alalm, M.G., Awfa, D., Johnson, M.S., Yoshimura, C., 2020. Modeling the degradation and disinfection of water pollutants by photocatalysts and composites: a critical review. Sci. Total Environ. 698, 134197. https://doi.org/10.1016/j.scitotenv.2019.134197.

Ateia, M., Apul, O.G., Shimizu, Y., Muflihah, A., Yoshimura, C., Karanfil, T., 2017a. Elucidating adsorptive fractions of natural organic matter on carbon nanotubes. Environ. Sci. Technol. 51, 7101–7110. https://doi.org/10.1021/acs.est.7b01279.

Ateia, M., Koch, C., Jelavić, S., Hirt, A., Quinson, J., Yoshimura, C., Johnson, M., 2017b. Green and facile approach for enhancing the inherent magnetic properties of carbon nanotubes for water treatment applications. PloS One 12, e0180636. https://doi.org/10.1371/journal.pone.0180636.

Awfa, D., Ateia, M., Fujii, M., Johnson, M.S., Yoshimura, C., 2018. Photodegradation of pharmaceuticals and personal care products in water treatment using carbonaceous-TiO2 Composites : a critical review of recent literature. Water Res. 142, 1–77. https://doi.org/10.1016/j.watres.2018.05.036.

Awfa, D., Ateia, M., Fujii, M., Yoshimura, C., 2019. Novel magnetic carbon nanotube-TiO2 composites for solar light photocatalytic degradation of pharmaceuticals in the presence of natural organic matter. J. Water Process Eng. 31, 100836. https://doi.org/10.1016/j.jwpe.2019.100836.

Bekbolet, M., Sen-Kavurmaci, S., 2015. The effect of photocatalytic oxidation on molecular size distribution profiles of humic acid. Photochem. Photobiol. Sci. 14, 576–582. https://doi.org/10.1039/c4pp00262h.

Birben, N.C., Tomruk, A., Bekbolet, M., 2017. The role of visible light active TiO2 specimens on the solar photocatalytic disinfection of E. coli. Environ. Sci. Pollut. Res. 24, 12618–12627. https://doi.org/10.1007/s11356-016-7769-8.

Brame, J., Long, M., Li, Q., Alvarez, P., 2015. Inhibitory effect of natural organic matter or other background constituents on photocatalytic advanced oxidation processes: mechanistic model development and validation. Water Res. 84,

362–371. https://doi.org/10.1016/j.watres.2015.07.044.
Cai, Q., Hu, J., 2017. Decomposition of sulfamethoxazole and trimethoprim by continuous UVA/LED/TiO2 photocatalysis: decomposition pathways, residual antibacterial activity and toxicity. J. Hazard Mater. 323, 527–536. https://doi.org/10.1016/j.jhazmat.2016.06.006.
Carbonaro, S., Sugihara, M.N., Strathmann, T.J., 2013. Continuous-flow photocatalytic treatment of pharmaceutical micropollutants: activity, inhibition, and deactivation of TiO2 photocatalysts in wastewater effluent. Appl. Catal. B Environ. 129, 1–12. https://doi.org/10.1016/j.apcatb.2012.09.014.
Cardoso, O., Porcher, J.M., Sanchez, W., 2014. Factory-discharged pharmaceuticals could be a relevant source of aquatic environment contamination: review of evidence and need for knowledge. Chemosphere 115, 20–30. https://doi.org/10.1016/j.chemosphere.2014.02.004.
Carstea, E.M., Bridgeman, J., Baker, A., Reynolds, D.M., 2016. Fluorescence spectroscopy for wastewater monitoring: a review. Water Res. 95, 205–219. https://doi.org/10.1016/j.watres.2016.03.021.
Coble, P.G., 1996. Characterization of marine and terrestrial DOM in the seawater using exciting-emission matrix.pdf 51, 325-346. https://doi.org/10.1016/0304-4203(95)00062-3.
Del Vecchio, R., Blough, N.V., 2002. Photobleaching of chromophoric dissolved organic matter in natural waters: kinetics and modeling. Mar. Chem. 78, 231–253. https://doi.org/10.1016/S0304-4203(02)00036-1.
Deng, J., Shao, Y., Gao, N., Xia, S., Tan, C., Zhou, S., Hu, X., 2013. Degradation of the antiepileptic drug carbamazepine upon different UV-based advanced oxidation processes in water. Chem. Eng. J. 222, 150–158. https://doi.org/10.1016/j.cej.2013.02.045.
Dickenson, E.R.V., Snyder, S.A., Sedlak, D.L., Drewes, J.E., 2011. Indicator compounds for assessment of wastewater effluent contributions to flow and water quality. Water Res. 45, 1199–1212. https://doi.org/10.1016/j.watres.2010.11.012.
Dickenson, E.R.V., Drewes, J.E., Sedlak, D.L., Wert, E.C., Snyder, S.A., 2009. Applying surrogates and indicators to assess removal efficiency of trace organic chemicals during chemical oxidation of wastewaters. Environ. Sci. Technol. 43, 6242–6247. https://doi.org/10.1021/es803696y.
Doll, T.E., Frimmel, F.H., 2005. Photocatalytic degradation of carbamazepine, clofibric acid and iomeprol with P25 and Hombikat UV100 in the presence of natural organic matter (NOM) and other organic water constituents. Water Res. 39, 403–411. https://doi.org/10.1016/j.watres.2004.09.016.
Doong, R.A., Chen, C.H., Maithreepala, R.A., Chang, S.M., 2001. The influence of pH and cadmium sulfide on the photocatalytic degradation of 2-chlorophenol in titanium dioxide suspensions. Water Res. 35, 2873–2880. https://doi.org/10.1016/S0043-1354(00)00580-7.
Drosos, M., Ren, M., Frimmel, F.H., 2015. The effect of NOM to TiO2: interactions and photocatalytic behavior. Appl. Catal. B Environ. 165, 328–334. https://doi.org/10.1016/j.apcatb.2014.10.017.
Ersan, G., Apul, O.G., Perreault, F., Karanfil, T., 2017. Adsorption of organic contaminants by graphene nanosheets: a review. Water Res. 126 https://doi.org/10.1016/j.watres.2017.08.010.
Ferrari, B., Paxéus, N., Giudice, R. Lo, Pollio, A., Garric, J., 2003. Ecotoxicological impact of pharmaceuticals found in treated wastewaters: study of carbamazepine, clofibric acid, and diclofenac. Ecotoxicol. Environ. Saf. 55, 359–370. https://doi.org/10.1016/S0147-6513(02)00082-9.
Guerard, J.J., Miller, P.L., Trouts, T.D., Chin, Y.P., 2009. The role of fulvic acid composition in the photosensitized degradation of aquatic contaminants. Aquat. Sci. 71, 160–169. https://doi.org/10.1007/s00027-009-9192-4.
Haroune, L., Salaun, M., Ménard, A., Legault, C.Y., Bellenger, J.P., 2014. Photocatalytic degradation of carbamazepine and three derivatives using TiO2 and ZnO: effect of pH, ionic strength, and natural organic matter. Sci. Total Environ. 475, 16–22. https://doi.org/10.1016/j.scitotenv.2013.12.104.
Jallouli, N., Pastrana-Martínez, L.M., Ribeiro, A.R., Moreira, N.F.F., Faria, J.L., Hentati, O., Silva, A.M.T., Ksibi, M., 2018. Heterogeneous photocatalytic degradation of ibuprofen in ultrapure water, municipal and pharmaceutical industry wastewaters using a TiO2/UV-LED system. Chem. Eng. J. 334, 976–984. https://doi.org/10.1016/j.cej.2017.10.045.
Keen, O.S., McKay, G., Mezyk, S.P., Linden, K.G., Rosario-Ortiz, F.L., 2014. Identifying the factors that influence the reactivity of effluent organic matter with hydroxyl radicals. Water Res. 50, 408–419. https://doi.org/10.1016/j.watres.2013.10.049.
Kohl, A., Golan, N., Cinnamon, Y., Genin, O., Chefetz, B., Sela-Donenfeld, D., 2019. A proof of concept study demonstrating that environmental levels of carbamazepine impair early stages of chick embryonic development. Environ. Int. 129, 583–594. https://doi.org/10.1016/j.envint.2019.03.064.
Koli, V.B., Dhodamani, A.G., Raut, A.V., Thorat, N.D., Pawar, S.H., Delekar, S.D., 2016. Visible light photo-induced antibacterial activity of TiO2-MWCNTs nanocomposites with varying the contents of MWCNTs. J. Photochem. Photobiol. Chem. 328, 50–58. https://doi.org/10.1016/j.jphotochem.2016.05.016.
Lado Ribeiro, A.R., Moreira, N.F.F., Li Puma, G., Silva, A.M.T., 2019. Impact of water matrix on the removal of micropollutants by advanced oxidation technologies. Chem. Eng. J. 363, 155–173. https://doi.org/10.1016/j.cej.2019.01.080.
Lee, E., Shon, H.K., Cho, J., 2014. Role of wetland organic matters as photosensitizer for degradation of micropollutants and metabolites. J. Hazard Mater. 276, 1–9. https://doi.org/10.1016/j.jhazmat.2014.05.001.
Lee, Y.P., Fujii, M., Kikuchi, T., Natsuike, M., Ito, H., Watanabe, T., Yoshimura, C., 2017a. Importance of allochthonous and autochthonous dissolved organic matter in Fe(II) oxidation: a case study in Shizugawa Bay watershed, Japan. Chemosphere 180, 221–228. https://doi.org/10.1016/j.chemosphere.2017.04.008.
Lee, Y.P., Fujii, M., Kikuchi, T., Terao, K., Yoshimura, C., 2017b. Variation of iron redox kinetics and its relation with molecular composition of standard humic substances at circumneutral pH. PloS One 12, 1–21. https://doi.org/10.1371/journal.pone.0176484.
Li, S., Hu, J., 2018. Transformation products formation of ciprofloxacin in UVA/LED and UVA/LED/TiO2systems: impact of natural organic matter characteristics. Water Res. 132, 320–330. https://doi.org/10.1016/j.watres.2017.12.065.
Lv, J., Li, D., Luo, L., Wu, T., Zhang, S., 2017. Molecular transformation of natural and anthropogenic dissolved organic matter under photo-irradiation in the presence of nano TiO2. Water Res. 125, 201–208. https://doi.org/10.1016/j.watres.2017.08.051.
Meng, Y., Wang, Y., Han, Q., Xue, N., Sun, Y., Gao, B., Li, Q., 2016. Trihalomethane (THM) formation from synergic disinfection of biologically treated municipal wastewater: effect of ultraviolet (UV) irradiation and titanium dioxide photocatalysis on dissolve organic matter fractions. Chem. Eng. J. 303, 252–260. https://doi.org/10.1016/j.cej.2016.05.141.
Michael-Kordatou, I., Michael, C., Duan, X., He, X., Dionysiou, D.D., Mills, M.A., Fatta-Kassinos, D., 2015. Dissolved effluent organic matter: characteristics and potential implications in wastewater treatment and reuse applications. Water Res. 77, 213–248. https://doi.org/10.1016/j.watres.2015.03.011.
Miklos, D.B., Remy, C., Jekel, M., Linden, K.G., Drewes, J.E., Hübner, U., 2018. Evaluation of advanced oxidation processes for water and wastewater treatment – a critical review. Water Res. 139, 118–131. https://doi.org/10.1016/j.watres.2018.03.042.
Miranda, S.M., Romanos, G.E., Likodimos, V., Marques, R.R.N., Favvas, E.P., Katsaros, F.K., Stefanopoulos, K.L., Vilar, V.J.P., Faria, J.L., Falaras, P., Silva, A.M.T., 2014. Pore structure, interface properties and photocatalytic efficiency of hydration/dehydration derived TiO2/CNT composites. Appl. Catal. B Environ. 147, 65–81. https://doi.org/10.1016/j.apcatb.2013.08.013.
Moran, M.A., Sheldon, W.M., Zepp, R.G., 2000. Carbon loss and optical property changes during long-term photochemical and biological degradation of estuarine dissolved organic matter. Limnol. Oceanogr. 45, 1254–1264. https://doi.org/10.4319/lo.2000.45.6.1254.
Phong, D.D., Hur, J., 2016. Non-catalytic and catalytic degradation of effluent dissolved organic matter under UVA-and UVC-irradiation tracked by advanced spectroscopic tools. Water Res. 105, 199–208. https://doi.org/10.1016/j.watres.2016.08.068.
Phong, D.D., Hur, J., 2015. Insight into photocatalytic degradation of dissolved organic matter in UVA/TiO 2 systems revealed by fluorescence EEM-PARAFAC. Water Res. 87, 119–126. https://doi.org/10.1016/j.watres.2015.09.019.
Raeke, J., Lechtenfeld, O.J., Seiwert, B., Meier, T., Riemenschneider, C., Reemtsma, T., 2017. Photochemically induced bound residue formation of carbamazepine with dissolved organic matter. Environ. Sci. Technol. 51, 5523–5530. https://doi.org/10.1021/acs.est.7b00823.
Ren, M., Drosos, M., Frimmel, F.H., 2018. Inhibitory effect of NOM in photocatalysis process: explanation and resolution. Chem. Eng. J. 334, 968–975. https://doi.org/10.1016/j.cej.2017.10.099.
Rioja, N., Zorita, S., Peñas, F.J., 2016. Effect of water matrix on photocatalytic degradation and general kinetic modeling. Appl. Catal. B Environ. 180, 330–335. https://doi.org/10.1016/j.apcatb.2015.06.038.
Rodríguez, F.J., Schlenger, P., García-Valverde, M., 2014. A comprehensive structural evaluation of humic substances using several fluorescence techniques before and after ozonation. Part I: structural characterization of humic substances. Sci. Total Environ. 476–477, 718–730. https://doi.org/10.1016/j.scitotenv.2013.11.150.
Shimabuku, K.K., Kennedy, A.M., Mulhern, R.E., Summers, R.S., 2017. Evaluating activated carbon adsorption of dissolved organic matter and micropollutants using fluorescence spectroscopy. https://doi.org/10.1021/acs.est.6b04911.
Sousa, J.C.G., Ribeiro, A.R., Barbosa, M.O., Pereira, M.F.R., Silva, A.M.T., 2018. A review on environmental monitoring of water organic pollutants identified by EU guidelines. J. Hazard Mater. 344, 146–162. https://doi.org/10.1016/j.jhazmat.2017.09.058.
Vishnuganth, M.A., Remya, N., Kumar, M., Selvaraju, N., 2016. Photocatalytic degradation of carbofuran by TiO2-coated activated carbon: model for kinetic, electrical energy per order and economic analysis. J. Environ. Manag. 181, 201–207. https://doi.org/10.1016/j.jenvman.2016.06.016.
Wang, Y., Roddick, F.A., Fan, L., 2017. Direct and indirect photolysis of seven micropollutants in secondary effluent from a wastewater lagoon. Chemosphere 185, 297–308. https://doi.org/10.1016/j.chemosphere.2017.06.122.
Woan, K., Pyrgiotakis, G., Sigmund, W., 2009. Photocatalytic carbon-nanotube-TiO $_2$ composites. Adv. Mater. 21, 2233–2239. https://doi.org/10.1002/adma.200802738.
Yan, S., Yao, B., Lian, L., Lu, X., Snyder, S.A., Li, R., Song, W., 2017. Development of fluorescence surrogates to predict the photochemical transformation of pharmaceuticals in wastewater effluents. Environ. Sci. Technol. https://doi.org/10.1021/acs.est.6b05251 acs.est. 6b05251.
Yang, K., Xing, B., 2009. Adsorption of fulvic acid by carbon nanotubes from water. Environ. Pollut. 157, 1095–1100. https://doi.org/10.1016/j.envpol.2008.11.007.
Yao, Y., Li, G., Ciston, S., Lueptow, R.M., Gray, K.A., 2008. Photoreactive TiO2/carbon nanotube composites: synthesis and reactivity. Environ. Sci. Technol. 42, 4952–4957. https://doi.org/10.1021/es800191n.
Ye, Y., Bruning, H., Liu, W., Rijnaarts, H., Yntema, D., 2019. Effect of dissolved natural organic matter on the photocatalytic micropollutant removal performance of TiO2 nanotube array. J. Photochem. Photobiol. Chem. 371, 216–222. https://doi.org/10.1016/j.jphotochem.2018.11.012.

Yuan, C., Hung, C.H., Li, H.W., Chang, W.H., 2016. Photodegradation of ibuprofen by TiO2 co-doping with urea and functionalized CNT irradiated with visible light - effect of doping content and pH. Chemosphere 155, 471–478. https://doi.org/10.1016/j.chemosphere.2016.04.055.

Yuan, R., Zhu, Y., Zhou, B., Hu, J., 2018. Photocatalytic oxidation of sulfamethoxazole in the presence of TiO2: effect of matrix in aqueous solution on decomposition mechanisms. Chem. Eng. J. 359, 1527–1536. https://doi.org/10.1016/j.cej.2018.11.019.

Zhang, B., Zou, S., Cai, R., Li, M., He, Z., 2018a. Highly-efficient photocatalytic disinfection of Escherichia coli under visible light using carbon supported Vanadium Tetrasulfide nanocomposites. Appl. Catal. B Environ. 224, 383–393. https://doi.org/10.1016/j.apcatb.2017.10.065.

Zhang, P., Zhou, H., Li, K., Zhao, X., Liu, Q., Li, D., Zhao, G., 2018b. Occurrence of pharmaceuticals and personal care products, and their associated environmental risks in a large shallow lake in north China. Environ. Geochem. Health. https://doi.org/10.1007/s10653-018-0069-0.

Zhao, C., Wang, Z., Wang, C., Li, X., Wang, C.C., 2018. Photocatalytic degradation of DOM in urban stormwater runoff with TiO2 nanoparticles under UV light irradiation: EEM-PARAFAC analysis and influence of co-existing inorganic ions. Environ. Pollut. 243, 177–188. https://doi.org/10.1016/j.envpol.2018.08.062.

Zouzelka, R., Kusumawati, Y., Remzova, M., Rathousky, J., Pauporté, T., 2016. Photocatalytic activity of porous multiwalled carbon nanotube-TiO2 composite layers for pollutant degradation. J. Hazard Mater. 317, 52–59. https://doi.org/10.1016/j.jhazmat.2016.05.056.